Al-Khwarizmi Engineering Journal, Vol. 9, No. 1, P.P. 83-93 (2013)

Al-Khwarizmi Engineering Journal

Mechanical Properties and Corrosion Behavior of Low Carbon Steel Weldments

Rana A.Majed **Majid H. Abdulmajeed** **Mohamed Mahdy**

Department of Materials Engineering/ University of Technology

(Received 10 April 2012; accepted 18 February 2013)

Abstract

This research involves studying the mechanical properties and corrosion behavior of "low carbon steel" (0.077wt% C) before and after welding using Arc, MIG and TIG welding. The mechanical properties include testing of microhardness, tensile strength, the results indicate that microhardness of TIG, MIG welding is more than arc welding, while tensile strength in arc welding more than TIG and MIG.

The corrosion behavior of low carbon weldments was performed by potentiostat at scan rate $3mV.sec^{-1}$ in 3.5% NaCl to show the polarization resistance and calculate the corrosion rate from data of linear polarization by "Tafel extrapolation method". The results indicate that the TIG welding increase the corrosion current density and anodic Tafel slop, while decrease the polarization resistance compared with unwelded low carbon steel. Cyclic polarization were measured to show resistance of specimens to pitting corrosion and to calculate the forward and reveres potentials. The results show shifting the forward, reverse and pitting potentials toward active direction for weldments samples compared with unwelded sample.

Keywords: *Low carbon steel, Acr, MIG and TIG Welding, mechanical properties of weldments, corrosion behavior of weldments, Tafel extrapolation.*

1. Introduction

The corrosion behavior of carbon steel weldments is dependent on a number of factors. Consideration must be given to the compositional effects of low carbon steel and welding consumable and to the different welding processes used. Because carbon steels undergo metallurgical transformations across the weld and heat-affected zone (HAZ), microstructures and morphologies become important. A wide range of microstructures can be developed based on cooling rates, and these microstructures are dependent on energy input, preheat, metal thickness (heat sink effects), weld bead size, and reheating effects due to multiphase welding. As a result of their different chemical compositions and weld inclusions (oxides and sulfides), weld metal microstructures are usually significantly different from those of the HAZ and base metal. Similarly, corrosion behavior can also vary [1].

In addition, hardness levels will be the lowest for high heat inputs, such as those produced by submerged-arc weldments, and will be highest for low-energy weldments (with faster cooling rates) made by the shielded metal arc processes. Depending on the welding conditions, weld metal microstructures generally tend to be fine grained with basic flux and somewhat coarser with acid or rutile (TiO_2) flux compositions.

During welding, the base metal, HAZ, and underlying weld passes experience stresses due to thermal expansion and contraction. Upon solidification, rather high levels of residual stress remain as a result of weld shrinkage. Stress concentration effects as a result of geometrical discontinuities, such as weld reinforcement and lack of full weld penetration (dangerous because of the likelihood of crevice corrosion and the possibility of fatigue cracking), are also important because of the possibility of stress corrosion cracking SCC. Achieving full weld penetration, minimizing excessive weld reinforcement through

control of the welding process or technique, and grinding (a costly method) can be effective in minimizing these geometric effects. A stress-relieving heat treatment is effective in reducing internal weld shrinkage stress and metal hardness to safe levels in most cases.

This phenomenon has been observed in a wide range of aqueous environments. The common link being that the environments are fairly high in conductivity, while attack has usually, but not invariably, occurred at pH values below about 7 to 8. The reasons for localized weldment attack have not been fully defined. There is clearly a microstructural dependence, and studies on HAZs show corrosion to be appreciably more severe when the material composition and welding are such that hardened structures are formed. It has been known for many years that hardened steel may corrode more rapidly in acid conditions than fully tempered material, apparently because local microcathodes on the metal surface stimulate the cathodic hydrogen evolution reaction. On this basis, water treatments ensuring alkaline conditions should be less likely to induce HAZ corrosion, but even at pHs near 8, hydrogen ion (H^+) reduction can account for about 20% of the total corrosion current; pH values substantially above this level would be needed to suppress the effect completely [1].

It is probable that similar microstructural considerations also apply to the preferential corrosion of weld metal, but in this case, the situation is further complicated by the presence of deoxidation products, their type and number depending largely on the flux system employed. Consumable type plays a major role in determining weld metal corrosion rate, and the highest rates of metal loss are normally associated with shielded metal arc electrodes using a basic coating. In seawater, for example, the corrosion rate for a weld made using a basic-coated consumable may be three times as high as for weld metal from a rutile-coated consumable. Fewer data are available for submerged-arc weld metals, but it would appear than they are intermediate between basic and rutile shielded metal arc electrodes and that a corrosion rate above that of the base steel can be expected.

Galvanic-corrosion effects have also been observed and have caused unexpected failure of piping tank age and pressure vessels where the welds are anodic to the base metal. There is no doubt that residual welding stresses can cause SCC in environments in which such failure represents a hazard. This is the case for failure by both active path and hydrogen embrittlement mechanisms, and in the latter case, failure may be especially likely at low heat input welds because of the enhanced susceptibility of the hardened structures inevitably formed. Most SCC studies of welds in carbon and carbon-manganese steels have evaluated resistance to hydrogen-induced SCC, especially under sour (H_2S) conditions prevalent to the oil and gas industry [1].

2. Materials and Procedure

Commercial low carbon steel (chemical composition wt%: 0.077 C, 0.309 Mn, 0.003 Si, 0.0001 P, 0.021 S, 0.0001 Cr, 0.0002 Mo, 0.023 Cu, 0.0001 Ni, 0.003 V and Fe remain), have dimensions (20 x 20 x 3 mm) was used in this work. Three couples of samples were welded by "MIG" welding and the other three couples were welded by arc welding. During MIG welding argon gas was used with 100 Amp and 25 Volt was used and in the arc welding 120 Amp and 45 V was used.

In order to investigate the microstructure some of the welded pieces were ground using emery paper 100, 240, 320, 600, 800 1000 and 1200p before the heat treatment. Then they were polished by Alumina solution using "nitel solution" (98% alchohol-2% nitric acid) for 5 sec. The microstructure was studied under reflected light microscope.

After preparation the surface specimen, the micro hardness test was achieved, so the microhardness test is a test for mechanical hardness used particularly for very brittle materials or thin surface layer, where only a small indentation may be made for testing purposes. A pyramidal diamond point is pressed into the polished surface of the test material with a known force, for a specified well time, and the resulting indentation is measured using a microscope. The geometry of this indenter is an extended pyramid with the length to width ratio being (7:1) and respective face angles are 172 degrees for the long edge and 130 degrees for the short edge. The depth of the indentation can be approximated as 1/30 of the long dimension. We can obtain the result from the law [2]:

$$H = \frac{Load\ (kgf)}{Impression\ area\ (mm^2)} = \frac{P}{C_p L^2} \qquad ...(1)$$

Where L is length of indentation along its long axis, C_p is correction factor related to the shape of the indenter, ideally 0.070279 and P is load.

The advantages of the test are that only a very small sample of material is required, and that it is valid for a wide range of test forces. The main disadvantages are the difficulty of using a microscope to measure the indentation (with an accuracy of 0.5μm), and the time needed to prepare the sample and apply the indenter. So we got the micro hardness for three areas, base metal, HAZ metal and fusion zone with load (9.8kN) all values of microhardness were average of three measurements.

After micro hardness test, the tensile strength was measured for the samples, where the σ_{mas} or σ_u is indicated by the maxima of a stress-strain curve and, in general, indicates when necking will occur. This fracture will generally occur at the point of necking. After that heat treatment was done for the samples (Arc welding and MIG welding) using furnace at temperature 600 °C for time 15 minutes and the cooling was inside the furnace. The microstructure and micro hardness of the samples were measured after heat treatment too with a prior grinding and polishing.

To corrosion test, three samples of low carbon steel were welded using Arc, MIG and TIG welding to study effect of these treatments on the corrosion behavior of low carbon steel weldments. After welding all samples and as received specimens were mounted by hot mounting to insulate all but one side with an epoxy resin.

The open side was polished mechanically to a mirror finish, rinsed in distilled water and stored in desiccators. The electrolyte reference used was sea water (3.5% NaCl). Polarization experiments were performed in "WINKING M Lab 200" Potentiostat from Bank-Elektronik with electrochemical standard cell with provision for working electrode, auxiliary electrode (Pt electrode), and a Luggin capillary for connection with an saturated calomel electrode (SCE) reference electrode. Electrochemical measurements were performed with a potentiostat at a scan rate 3 $mV.sec^{-1}$.

The main results obtained were expressed in terms of the corrosion potentials (E_{corr}) and corrosion current density (i_{corr}) in addition to measure the "Tafel slops".

3. Results and Discussion

3.1. Mechanical Properties

Microscopic studies revealed that the base metal are coarser crystalline and elongated before heating becoming finer but still elongated after heating. The welding also affects the crystal size as the grains of the base become finer and equidimensional. However, the crystal size of the fusion zone are coarser and equidimensional before heating becoming elongated and oriented after heating (Fig. 1).

In Arc welding the micro hardness results of the base metal, heat affected zone and fusion zone, before heat treatment, are 188, 185 and 200 KN/mm^2 respectively. After heat treatment the micro hardness of the base metal, heat affected zone and fusion zone are 170, 186 and 190 KN/mm^2 respectively (Table 1). In MIG welding the micro hardness results of the base metal, heat affected zone and fusion zone, before heat treatment, are 187, 186 and 222 KN/mm^2 respectively. After heat treatment the micro hardness of the base metal, heat affected zone and fusion zone are 155, 163 and 236 KN/mm^2 respectively as shown in Table (1). But in TIG welding the micro hardness results of the base metal, heat affected zone and fusion zone, before heat treatment, are 185, 209 and 255 KN/mm^2 respectively. After heat treatment the micro hardness of the base metal, heat affected zone and fusion zone are 190, 200 and 236 KN/mm^2 respectively

In Arc welding the σ_{max} and the σ_y before heat treatment are 490 and 240 MPa respectively. The σ_{max} and the σ_y after heat treatment are 395 and 235 MPa respectively as shown in Table (2). While in MIG arc welding the σ_{max} and the σ_y before heat treatment are 395 and 390 MPa respectively. The σ_{max} and the σ_y after heat treatment are 320 and 235 MPa respectively as shown in Table (2). But In TIG welding the σ_{max} and the σ_y before heat treatment are 300 and 250 MPa respectively. The σ_{max} and the σ_y after heat treatment are 370 and 260 MPa respectively

It seems evident from the above mentioned tests that tensile strength and microhardness tests of the welded samples before and after heat treatment, has improved after welding. Both σ_y and σ_{max} (obtained directly from a digital apparatus attached to the tensile strength instrument). This behavior can probably attributed to the formation of ferrite in the inclusions, as the heating to high temperature led to the loss of carbon from the surface layer and thus decreasing hardness as shown in the photomicrographs.

The photomicrographs (Fig. (2)) revealed that most of the background consists of ferrite. The improvement of the mechanical properties, both microhardness and tensile strength, in the MIG

welding can be attributed to the fine-grained perlite microstructure owing to the quick cooling.

In brief, the arc welded pieces, both before and after heat treatment, lead to improvement in the tensile strength but on the expense of the microhardness, as it is less in comparison of the unwelded samples. This is the result of the ferrite formation in the inclusions. The MIG welded samples showed slightly lesser tensile strength results but considerable higher hardness owing to the higher formation of the perlite microstructure. The MIG welded samples showed lesser amount of defects than the arc welded samples.

Comparison of the microhardness test results reveals that the fusion zone of samples after heating in MIG and TIG welding is the highest reaching 236 KN/mm^2, whereas in arc welding the microhardness result after heat treatment is 190 KN/mm^2. Also the microhardness of the fusion zone in the Arc and TIG welding decreases from 200 to 190 KN/mm^2 and from 255 to 236 KN/mm^2 respectively after heat treatment whereas it increases in the MIG welding from 222 to 236 KN/mm^2.

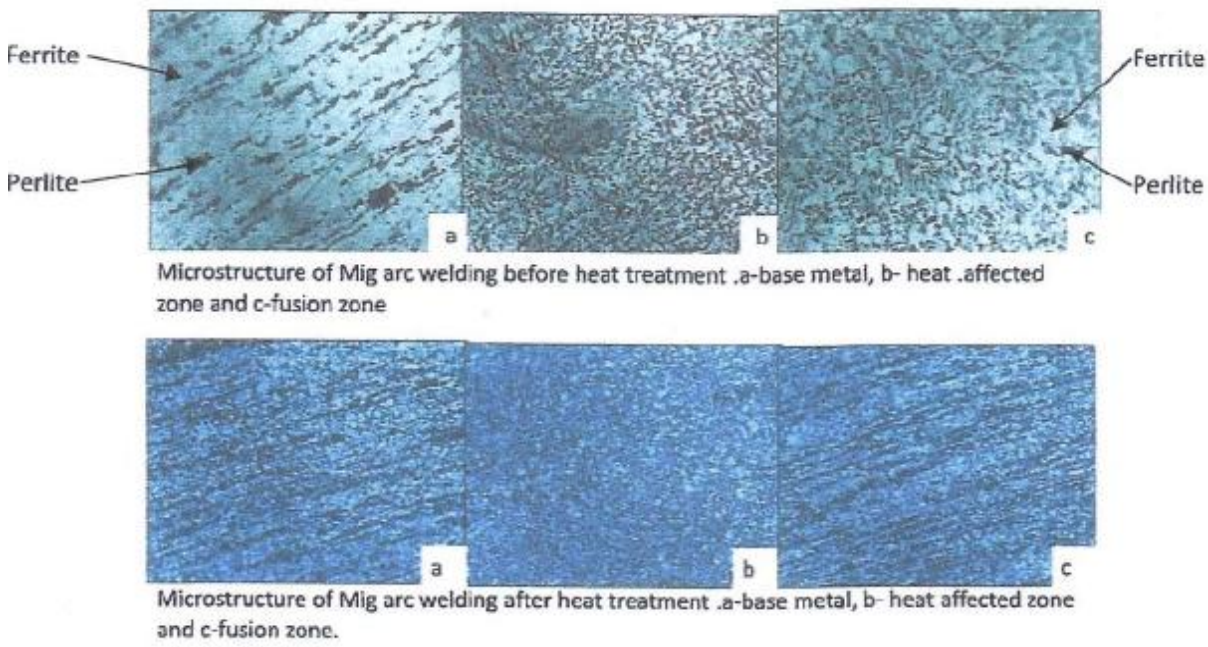

Fig. 1. Photomicrographs showing the Microstructures of the MIG arc Welded Samples Showing the Base Metal, the Heat Affected Zone and the Fusion Zone, 250x.

Table 1,
Results of the Microhardness of the Arc, MIG and TIG Welding before and after Heat Treatment.

Process	Base metal zone HV KN/mm^2	Heat affected zone HV KN/mm^2	Fusion zone HV KN/mm^2
Arc welding before heat treatment	188	185	200
Arc welding after heat treatment	170	186	190
MIG welding before heat treatment	187	186	222
MIG welding after heat treatment	155	163	236
TIG welding before heat treatment	185	209	255
TIG welding after heat treatment	190	200	236

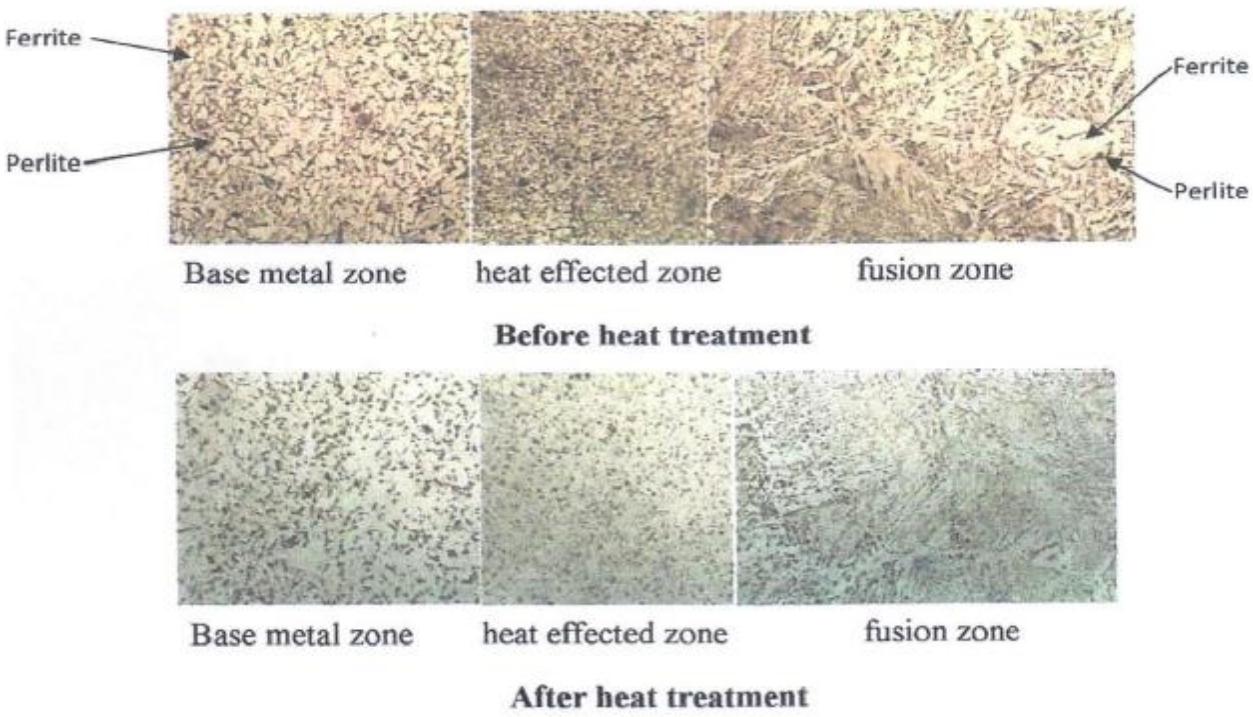

Fig. 2. Photomicrographs showing the Microstructures of the arc Welded Samples showing the Base Metal, the Heat Affected Zone and the Fusion Zone, 250x.

Table 2,
Results of the Tensile Strength of the Arc, MIG and TIG Welding before and after Heat Treatment.

Process	σ_{max}	σ_y
Arc welding before heat treatment	490	240
Arc welding after heat treatment	395	235
MIG welding before heat treatment	390	395
MIG welding after heat treatment	320	235
TIG welding before heat treatment	300	250
TIG welding after heat treatment	370	260

3.2. Corrosion Behavior

The variation of "open circuit potential" (OCP) with time was shown in the Figure (3) for unwelded and welded low carbon steel samples in 3.5% NaCl. The OCP-time measurement is considered as an important parameter for evaluating the stability of the passive film of the specimens. The data in Table (3) indicate that all low carbon steel weldments shift the open circuit potential (E_{oc}) toward active direction. Thus sample of unwelded low carbon steel thermodynamically less tendency to corrosion. The behavior of weldments gives unstable surface/electrolyte interaction compared with the sample without welding through the variation of potential with time.

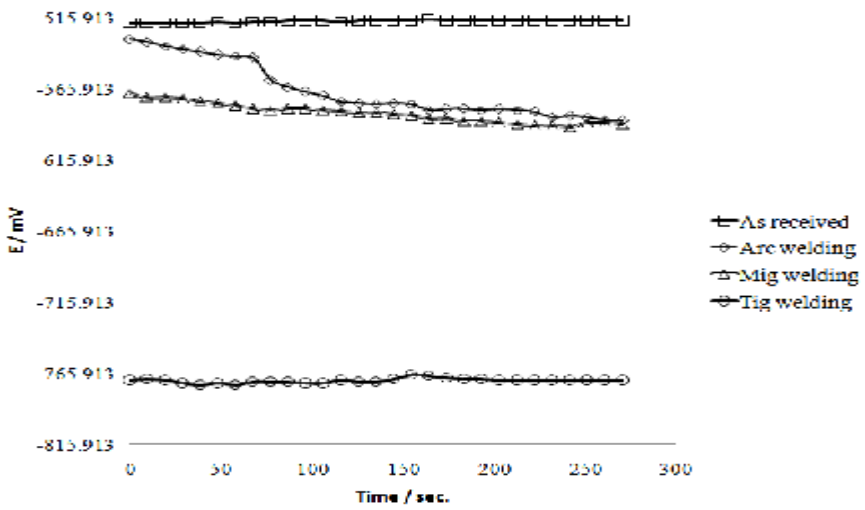

Fig. 3. Variation of Potentials with Time for as Received and Weldedlow Carbon Steel Alloy in 3.5% NaCl .

Table 3,
Corrosion Parameters of as Received and welded Specimens in Sea Water (3.5% NaCl) at Room Temperature.

Specimens	**Open circuit potential ($-E_{oc}$/mV)**	**Corrosion potential ($-E_{corr}$/mV)**	**Corrosion current density (i_{corr}/μA.cm^{-2})**	**Tafel slop (mV.dec^{-1}) $-b_c$**	**$+b_a$**	**Polar. resistance (R_p/Ω.cm^2)**
As received	518	516.3	21.45	124.8	72.80	0.9320
Welded with arc	589	635.4	14.26	126.7	91.9	1.6240
Welded with MIG	592	604.5	17.41	126.2	61.0	1.0270
Welded with TIG	765	790.9	24.13	96.60	94.5	0.8596

Linear polarization of unwelded and weldments show in Figs. (4) to (7) respectively. These figures show the cathodic and anodic behavior of samples, the cathodic reaction represent the reduction of oxygen according to the following reaction:

$O_2 + 4e + 2H_2O \rightarrow 4OH^-$

While the oxidation of iron represents the anodic reaction as follow:

$Fe \rightarrow Fe^{2+} + 2e$

The data of potentiodynamic polarization were listed in Table (3). These data show that the corrosion potentials (E_{corr}) values for weldments shift toward active direction compared with unwelded low carbon steel, and the sequence of negativity of corrosion potentials as follow: - **E_{corr}** TIG welding > Arc welding > MIG welding.

The effect of welding on the corrosion current density (i_{corr}) values indicate that the arc and MIG welding decrease the value of corrosion current density of low carbon steel without welding, while the TIG welding increases the corrosion current density. The values of cathodic Tafel slopes (b_c) show little increases in the case of arc and MIG welding, while decreases for TIG welding. But the anodic "Tafel slope" (b_a) increases in Arc and TIG welding and decrease for MIG welding sample.

The polarization resistance (R_p) can be determined from the Tafel slopes and according to Stern- Geary equation [3,4]:

$$R_p = \left(\frac{dE}{di}\right)_{i=0} = \frac{b_a . b_c}{2.303\ (b_a + b_c)\ i_{corr}} \quad \ldots.(2)$$

The results indicate increase in case of Arc and MIG welding and decreasing the polarization resistance for TIG welding sample compared with sample without welding.

Cyclic polarization measurements were carried out in order to determine the initiation and propagation of local corrosion, which is associated with the breakdown of passive protective film.

The breakdown potential (E_{br}) is the one at which the anodic current increases considerably with applied potential. The potential, at which the hysteresis loop is completed upon reverse polarization scan, is known as the protective potential or repassivation potential.

Breakdown potential is a sign of local corrosion but the measure of pitting susceptibility is the difference between the breakdown potential and the repassivation one. The protection potential represents the potential at the intersection of hysteresis curve with passive domain. Below this potential the propagation of existing localized corrosion will not occur.

If the difference between breakdown and the repassivation potential is increasing, the chance in the appearance of pitting is greater and its propagation in depth is more intense. In other words, the hysteresis loop increases as the susceptibility of material to corrosion increases.

The cyclic polarization of unwelded and weldments indicated in Fig. (8) to (11) in 3.5% NaCl. These figures show that the reverse scan starts right of the forward scan curve, that is, towards the high current density region.

This type of cyclic polarization curve is known to be less resist to localized corrosion. The potentials for the forward and reverse scan are more negative than that of unwelded sample, in addition to pitting potentials (E_{pit}) values which are more negative than pitting potential of as received sample. The data of forward and reverse scan are listed in the Table (4). Generally, the data of corrosion test indicate that the welding increase the ability of materials to corrode. The tendency of forward, reverse and pitting potentials for weldments take the following sequence:

$-E_{for.}$, $-E_{rev.}$ *and* $-E_{pit.}$ TIG welding > Arc welding >MIG welding

Weldments can experience all the classical forms of corrosion, but they are particularly susceptible to those affected by variations in microstructure and composition. Specifically, galvanic corrosion, pitting, stress corrosion, intergranular corrosion, hydrogen cracking, and microbiologically influenced corrosion must be considered when designing welded structures. Galvanic Couples, although some alloys can be autogenously welded, filler metals are more commonly used. The use of filler metals with compositions different from the base material may produce an electrochemical potential difference that makes some regions of the weldment more active.

For the majority of aluminum alloys, the weld metal and the HAZ become nobler relative to the base metal [5]. Certain aluminum alloys, however, form narrow anodic regions in the HAZ and are prone to localized attack. Alloys 7005 and 7039 are particularly susceptible to this problem. There are a number of other common weld deposit/base metal combinations that are known to form galvanic couples. It is common practice to use austenitic stainless steel welding consumables for field repair of heavy machinery, particularly those fabricated from high-strength low-alloy steel. This practice leaves a cathodic stainless steel weld deposit in electrical contact with the steel. In the presence of corrosive environments, hydrogen is generated at the austenitic weld metal cathode, which is capable of maintaining high hydrogen content without cracking. However, the cathodic behavior of the austenitic weld deposit may increase the susceptibility for (SCC) in the HAZ of the high-strength steel. A 40% thermal expansion mismatch between the austenitic stainless steel and ferritic base metal produces a significant residual stress field in the weldment; this residual stress field also contributes to cracking susceptibility. A similar, but more localized, behavior may explain the correlation between stress corrosion cracking susceptibility and the presence of retained austenite in high-strength steel weld deposits.

Another common dissimilar metal combination involves the use of high-nickel alloys for weld repair of cast iron. Fe-55Ni welding electrodes are used to make weld deposits that can hold in solid solution many of the alloying elements common to cast iron. Furthermore, weld deposits made with Fe-55Ni welding consumables have an acceptable thermal expansion match to the cast iron. Because cast iron is anodic to the high-nickel weld deposit, corrosive attack occurs in the cast iron adjacent to the weld deposit. It is suggested that cast iron welds made with high-nickel deposits be coated (painted) to reduce the susceptibility to selective corrosion attack.

Plain carbon steel weldments can also exhibit galvanic attack. For example, the E6013 welding electrode is known to be highly anodic to A285 base metal in a seawater environment [6]. It is important to select a suitable filler metal when an application involves a harsh environment.

Welding can reduce base metal corrosion resistance in aggressive environments. In welding,

heat is generated that produces a temperature gradient in the base metal, i.e. the HAZ. Welding may a so induce residual stresses in the weld area which in certain environments can lead to SCC. One of the early corrosion problems related to welding was intergranular attack, IGA, in the weld HAZ. In the temperature range of about 800°F to 1650°F (425°C to 900°C), carbon combines with chromium to form chromium carbides at the grain boundaries. The area adjacent to the carbides is depleted in chromium. When the carbide network is continuous, the low chromium envelope around grains may be selectively attacked, resulting in intergranular corrosion [7].

Table 4,
Data of Cyclic Polarization of as Received and Welded Specimens in Sea Water (3.5% NaCl) at Room Temperature.

Specimens	Forward potential ($-E_{for}$/mV)	Reverse potential ($-E_{rev}$/mV)	Pitting potential ($-E_{pit}$/mV)
As received	571.4	524.5	478.3
Welded with arc	689.6	673.8	666.3
Welded with MIG	622.7	606.2	589.1
Welded with TIG	790.3	779.3	771.8

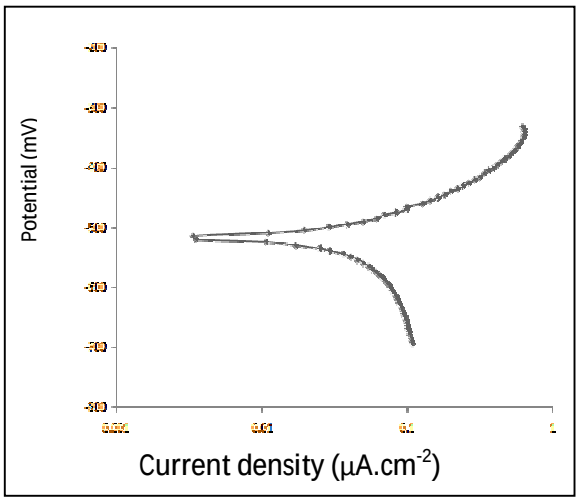

Fig. 4. Linear Polarization for Unwelded Low Carbon Steel in 3.5%NaCl.

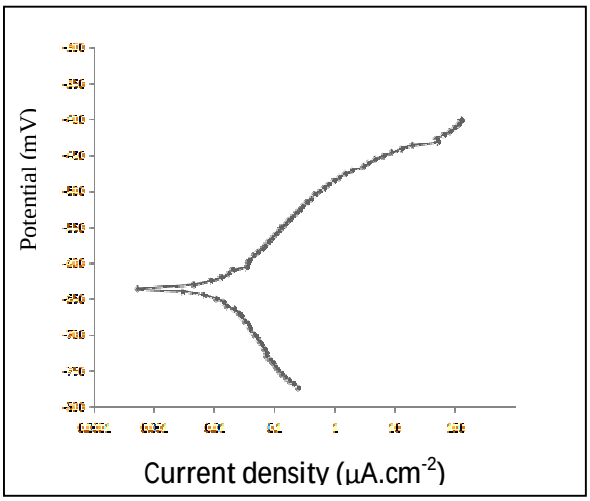

Fig. 5. Linear Polarization for Arc welded low carbon Steel in 3.5%NaCl.

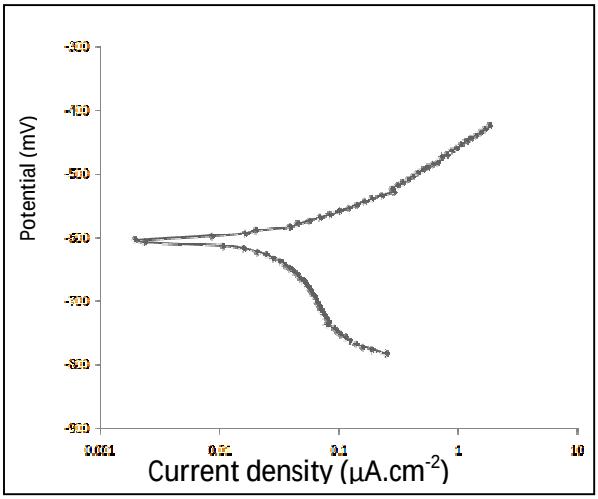

Fig. 6. Linear Polarization for MIG Welded low Carbon Steel in 3.5%NaCl.

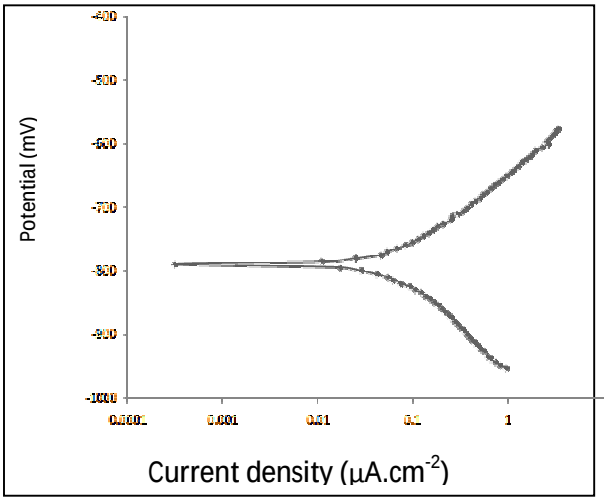

Fig. 7. Linear Polarization for TIG Welded Low Carbon Steel in 3.5%NaCl.

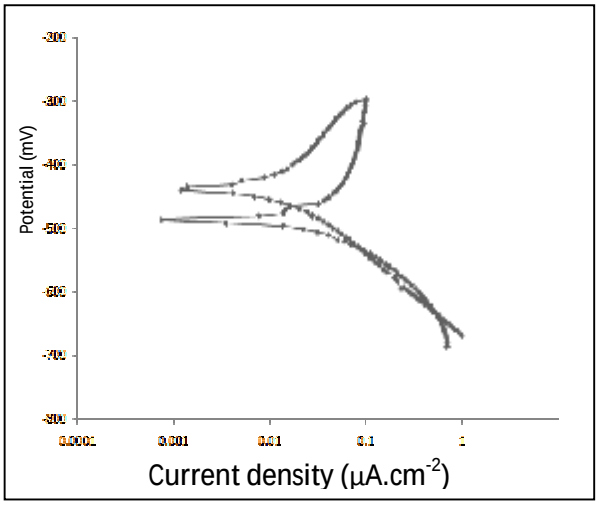

Fig. 8. Cyclic Polarization for as Received Low Carbon Steel in 3.5%NaCl.

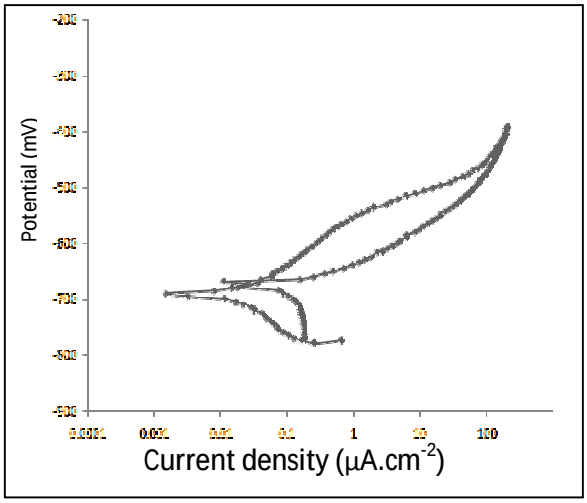

Fig. 9. Cyclic Polarization for Arc Welded Low Carbon Steel in 3.5%NaCl.

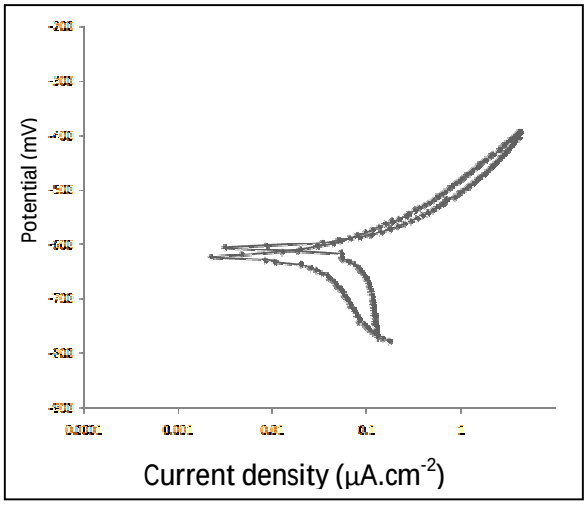

Fig. 10. Cyclic Polarization for MIG Welded Low Carbon Steel in 3.5%NaCl.

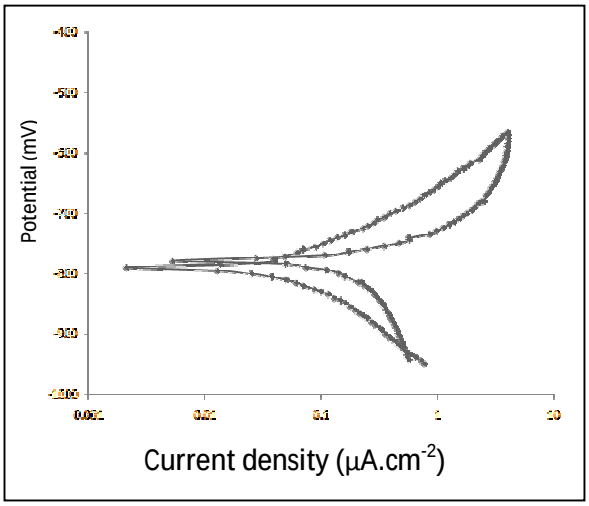

Fig. 11. Cyclic Polarization for TIG Welded Low Carbon Steel in 3.5%NaCl.

4. Conclusion

The following conclusions can be drawn from the present study:

1. The Arc welded pieces, both before and after heat treatment, lead to improvement in the tensile strength but on the expense of the microhardness, as it is less in comparison of the unwelded sample. This is the result of the ferrite formation in the inclusions.
2. The MIG and TIG welded samples showed slightly lesser tensile strength results but considerable higher hardness owing to the higher formation of the perlite microstructure.
3. The MIG and TIG welded samples showed lesser amount of defects than the Arc welded samples.
4. The welding enhances the corrosion of low carbon steel in sea water, and TIG welded more liable to corrosion compared with Arc and MIG welding.
5. The TIG welded samples has more negative corrosion, forward, reverse, pitting potentials.
6. The TIG welded samples has the corrosion current density and the highest anodic "Tafel slope" and the lowest polarization resistance than other welded samples.

5. References

[1] C.G. Arnold, "Galvanic Corrosion Measurement of Weldments," Paper 71, presented at Corrosion/ 80, Chicago, IL, National Association of Corrosion Engineers, March 1980

[2] J. R. Davis, "Metal Handbook", second edition (1998).

[3] Stern, M., Method for Determining Corrosion Rates from Linear Polarization Data, Corrosion, Vol.14, No.9, 1958,P.440–444.

[4] Stern M., and Geary, A. L., Electrochemical Polarization I: A theoretical Analysis of the Slope of Polarization Curves, *Journal of the Electrochemical Society*, Vol. 104, No. 1, 1957, P.559–563.

[5] J.E. Hatch, Ed., Aluminum: properties and physical metallurgy, ASM International, 1984, p.283.

[6] C.A. Arnold, "Galvanic corrosion measurement of weldments", presented at NACE corrosion/ 80, Chicago, March 1980.

[7] Basic understanding of weld corrosion, 2006 ASM International, www. asminternational.org.

الخواص الميكانيكية وسلوك التآكل لملحومات الفولاذ واطيء الكاربون

رنا عفيف مجيد ماجد حميد عبد المجيد محمد مهدي جبار

قسم هندسة المواد/ الجامعة التكنولوجية

الخلاصة

يتضمن هذا البحث دراسة بعض الخواص الميكانيكية وسلوك التاكل لملحومات الفولاذ واطيء الكاربون باستخدام لحام القوس الكهربائي ولحام القوس المعدني المحمي بالغاز الخامل واللحام بقوس التنجستن المحمي بالغاز الخامل، وقد تضمنت الخواص الميكانيكية كلاً من اختبارالصلادة المجهرية واختبارات مقاومة الشد، وتشير النتائج الى ان لحام قوس التنجستن المحمي بالغاز الخامل ولحام القوس المعدني المحمي بالغاز الخامل على التوالي اكثر صلادة من لحام القوس الكهربائي، بينما مقاومة الشد في لحام القوس الكهربائي اكثر مما هي في لحام قوس التنجستن المحمي بالغاز الخامل ولحام القوس المعدني المحمي بالغاز الخامل.

وقد اجريت تجارب التاكل باستخدام "المجهاد الساكن" بمعدل مسح ٣ ملي فولت لكل ثانية في ماء البحر ٣.٥% كلوريد الصوديوم لحساب متغيرات التاكل باستخدام "طريقة تافل الاستقرائية". وقد بينت نتائج التاكل بان اللحام بقوس التنجستن المحمي بالغاز الخامل يزيد الميل لحصول التاكل من خلال ارتفاع قيمة كثافة التيار و"ميل تافل الانودي" وكذلك النفص في مقاومة الاستقطاب مقارنة بالعينة غير الملحومة.

لقد اجري "المسح الحلقي" لمعرفة مدى مقاومة العينات الملحومة لتاكل التنقر، وقد دلت النتائج على ان جهود المسح الامامي والعكسي والتنقر كانت اكثر سالبية مقارنة بالعينة غير الملحومة.